1972-03

Some numerical aspects of developing an operational primitive-equation model for the tropics.

Langland, Rodger Alfred

Monterey, California. Naval Postgraduate School

SOME NUMERICAL ASPECTS OF DEVELOPING AN OPERATIONAL PRIMITIVE-EQUATION MODEL FOR THE TROPICS

Rodger Alfred Langland

NAVAL POSTGRADUATE SCHOOL
Monterey, California

THESIS

Some Numerical Aspects of Developing
an
Operational Primitive-Equation Model
for the Tropics

by

Rodger Alfred Langland

Thesis Advisor: R. L. Elsberry

March 1972

Approved for public release; distribution unlimited.

Some Numerical Aspects of Developing an Operational Primitive-Equation Model for the Tropics

by

Rodger Alfred Langland
Lieutenant, United States Navy
B.S., University of Washington, 1966

Submitted in partial fulfillment of the requirements for the degree of

MASTER OF SCIENCE IN METEOROLOGY

from the

NAVAL POSTGRADUATE SCHOOL
March 1972

ABSTRACT

A barotropic primitive equation model on a global tropical grid using operational real data is used to test various boundary conditions and methods of initialization including numerical variational analysis. Comparisons of forecast accuracy are made between staggered and non-staggered grids.

All prediction models produce better verification statistics than persistence, with the staggered grid verifying better than the full grid. This appears to be a result of two-gridlength noise being of greater magnitude in the full grid model. Less altering of individual synoptic systems occurs in the variational analysis initialization compared to two forms of the nonlinear balance equation. As a result, nondivergent variational analysis input fields to the prediction models result in the best verification values.

TABLE OF CONTENTS

LIST OF TABLES

LIST OF SYMBOLS

f	Coriolis parameter
Fx, Fy	Frictional terms of momentum equations
g	Acceleration of gravity
I	Grid index in x (west-east) direction
J	Grid index in y (south-north) direction
K	Grid index in vertical (pressure) direction
m	Mercator map factor
p	Pressure (independent variable)
R	Gas constant
q	Specific humidity
t	Time (independent variable)
u	Velocity component in x direction
v	Velocity component in y direction
x,y	Independent variables (west-east, south-north)
z	Height of constant pressure surface
α	NVA constant specifying dynamic tolerance
$\tilde{\alpha}$	NVA constant specifying wind tolerance
$\tilde{\beta}$	NVA constant specifying pressure tolerance
ζ	Vertical component of relative vorticity
θ	Potential temperature
ρ	Density of air
ϕ	Geopotential height
ψ	Stream function
ω	Velocity component in vertical (pressure) direction in x,y,p,t coordinate system

ACKNOWLEDGEMENT

The author wishes to extend his sincere appreciation to Professor R. L. Elsberry for the guidance he patiently provided during this research.

The author is also grateful to Professor R. T. Williams for his assistance during the course of this research.

In addition, the author wishes to express his thanks to Captain W. S. Houston, Jr. and the personnel of the Fleet Numerical Weather Central, Monterey, especially Dr. J. M. Lewis and Lieutenant G. W. Svenheim for the computer support provided.

I. INTRODUCTION

Numerical weather prediction in the tropics has developed slower than prediction in the mid-latitudes for many reasons. The lack of data and less understanding of the actual physical processes governing the circulations in the tropics are probably the major deterrents to progress. In recent years, the increase of meteorological data and increased understanding of the dynamics in the tropics have sparked interest in attempts at operational forecasting.

Tropical weather prediction can be approached on either a global band grid or a global grid. Certain characteristics of tropical prediction make the global band advantageous over the global grid. In mid-latitudes, much of the baroclinic energy exchange occurs on the long wave scale while in the tropics, the input of energy on the cumulus scale is also an important contributor to the dynamics. This complicates the global prediction by making the tropics a subset of the entire globe. In mid-latitude regions of the Northern Hemisphere, data are routinely available at all the mandatory levels as well as significant levels. In the tropics, data availability is a different story. Upper level data near 300 mb are available from aircraft reports combined with scarce conventional rawinsondes. Gradient level and surface level data are also routinely available in numbers approaching those necessary for input

to an operational model. However, the tropical regions are lacking in mid-tropospheric observations. The combination of a smaller scale of motion and the observational data available make data initialization in the tropics somewhat different than that in mid-latitudes. Reduction of the divergence equation to the balance equation, which is a generalized diagnostic equation used to relate wind and heights in mid-latitudes, is dependent upon a scale analysis in which the Rossby number is assumed less than one. This is not satisfied in the tropics however. Also, the optimum amount of divergence remaining in the initialized fields, which are used as input to a prediction model, may differ in the tropics from that in mid-latitudes.

As a result of the above considerations, Fleet Numerical Weather Central, Monterey now produces an operational wind and temperature analysis for a global band from 41S to 60N at eight levels ranging from the surface to 100 mb. A more detailed description is presented later in this thesis. This analysis is a potential input to the primitive equation prediction model. Steinbruck (1971) conducted preliminary experiments on this global band grid using climatological data. He investigated the properties of various boundary conditions on the primitive equation prediction model and various diagnositic balancing schemes, including numerical variational analysis (NVA) developed by Dr. J. M. Lewis (1972) for the global band.

The purpose of this thesis is to extend this research

to daily operational real data and to introduce a staggered grid system in an attempt to reduce memory and time requirements on the computer. A deliberate attempt is made to avoid introducing averaging and diffusion in order to produce as pure a forecast as possible and isolate true differences between boundary conditions and the various techniques for calculating initial data.

II. PRIMITIVE EQUATION PREDICTION MODEL

A. BASIC MODEL

A ten-layer primitive equation model, developed by Harrison (1970) and Elsberry and Harrison (1970, 1972), was used as a basis for the barotropic models used in these experiments. The equations for the ten-layer model are:

$$\frac{\partial u}{\partial t} = -L(u) + fv - m\frac{\partial \phi}{\partial x} + Fx \tag{1}$$

$$\frac{\partial v}{\partial t} = -L(v) - fu - m\frac{\partial \phi}{\partial y} + Fy \tag{2}$$

$$\frac{\partial \theta}{\partial t} = -L(\theta) + heat \tag{3}$$

$$\frac{\partial q}{\partial t} = -L(q) + moisture \tag{4}$$

$$\frac{\partial \phi_{1000}}{\partial t} = -L(\phi_{1000}) \tag{5}$$

$$\frac{\partial \omega}{\partial p} = -m^2 \left[\frac{\partial}{\partial x}\left(\frac{u}{m}\right) + \frac{\partial}{\partial y}\left(\frac{v}{m}\right)\right] \tag{6}$$

$$\Delta\phi = \hat{\theta}\, C_p\, \Delta \left(\frac{p}{1000}\right)^{R/C_p} \tag{7}$$

where

$$L(s) = m^2 \left[\frac{\partial}{\partial x}\left(\frac{us}{m}\right) + \frac{\partial}{\partial y}\left(\frac{vs}{m}\right)\right] + \frac{\partial}{\partial p}(\omega s) \tag{8}$$

and normal meteorological symbols are used with:

Δ = finite difference

$\hat{}$ = layer mean value

1000 = 1000 mb surface

m = map factor

S = general scalar dependent variable

L = advective operator

Linear stability is maintained by requiring the ratio of the space increment to the time increment be greater than the phase speed of the fastest waves, which are gravity waves. At 300 mb, and on the grid used, this time step is five minutes since the space increment near 60N is approximately 75 nautical miles.

All models use a forward time step in the first prediction step: $S^1 = S^o + \Delta t * \text{function } (S^o)$. All subsequent prediction steps use a leapfrog scheme where: $S^{n+1} = S^{n-1} + 2\,\Delta t * \text{function } (S^n)$.

B. NON-STAGGERED GRID BAROTROPIC PREDICTION MODEL

Because the prediction models to be discussed here are barotropic, Eqns. (3), (4) and (7) are not needed and since all prediction is done at the 300 mb level, Eqn. (5) becomes:

$$\frac{\partial \phi_{300}}{\partial t} = - m^2 \left[\frac{\partial}{\partial x}\left(\frac{u\phi}{m}\right) + \frac{\partial}{\partial y}\left(\frac{v\phi}{m}\right)\right]$$

The frictional terms in Eqns. (1) and (2) are neglected.

Input data to the models are the winds and geopotential at 300 mb.

The finite difference formulas are based on Arakawa's (1966) flux form. This form of differencing attempts to preclude nonlinear computational instability by requiring that the advective terms conserve the mean square of any advected quantity. Therefore, mean square kinetic energy

is conserved by the nonlinear terms and nonlinear instability is avoided. All horizontal derivatives are centered two grid mesh derivatives. The horizontal advective terms for a general variable S with J the index in the y direction and I the index in the x direction are written:

$$\frac{\partial}{\partial x}\left(\frac{Su}{m}\right)_{J,I} = \frac{\left(\frac{Su}{m}\right)_{J,I+1/2} - \left(\frac{Su}{m}\right)_{J,I-1/2}}{\Delta x}$$

$$= \frac{\left[\frac{S_{J,I+1} + S_{J,I}}{2}\right] \frac{1}{2}\left[\frac{u}{m}_{J,I+1} + \frac{u}{m}_{J,I}\right] - \left[\frac{S_{J,I} + S_{J,I-1}}{2}\right] \frac{1}{2}\left[\frac{u}{m}_{J,I} + \frac{u}{m}_{J,I-1}\right]}{\Delta x}$$

Note that this finite differencing only averages parameters over two grid points and one grid length.

C. STAGGERED GRID BAROTROPIC PREDICTION MODEL

Computation of space derivatives in finite difference form incorporates data from adjacent grid points. This prompted attempts at distributing the variables at alternating grid points in an attempt to reduce computer time and memory. This approach was first attempted by Eliassen (1956) and subsequently has been used by many investigators in various forms. The prediction and conservation equations on the staggered grid are the same as on the full grid. The staggered grid distribution used in the barotropic prediction model involves u and v winds at alternat-

ing points, ϕ and ω at diagonally alternating points as shown in Fig. 1. The Mintz-Arakawa general circulation model as described by Langlois and Kwok (1969) and an ocean circulation model by Haney (1971) also use this form of the staggered grid. This grid uses the least number of points possible and still retains the characteristic that the pressure gradient force is evaluated over the same space increment as in the non-staggered grid. Advective terms, however, involve a larger space increment.

The horizontal advective terms for a wind variable X are written:

$$\left(\frac{\partial}{\partial x}\left[\frac{Xu}{m}\right]\right)_{x=J,I} = \frac{\left(\frac{Xu}{m}\right)_{x=J,I+1/2} - \left(\frac{Xu}{m}\right)_{x=J,I-1/2}}{2\Delta x}$$

$$= \frac{\left[\frac{X_{J,I+1} + X_{J,I}}{2}\right]\frac{1}{2}\left[\left(\frac{u}{m}\right)_{J,I+1} + \left(\frac{u}{m}\right)_{J,I}\right] - \left[\frac{X_{J,I} + X_{J,I-1}}{2}\right]\frac{1}{2}\left[\left(\frac{u}{m}\right)_{J,I} + \left(\frac{u}{m}\right)_{J,I-1}\right]}{2\Delta x}$$

Refer to Fig. 1 for indexing. In a similar manner, the horizontal advection of geopotential (ϕ) takes the form:

$$\left(\frac{\partial}{\partial x}\left(\frac{\phi X}{m}\right)\right)_{0=J,I} = \frac{\left(\frac{\phi X}{m}\right)_{0=J,I+1/2} - \left(\frac{\phi X}{m}\right)_{0=J,I-1/2}}{2\Delta x}$$

$$= \frac{\left[\frac{\phi_{J,I+1} + \phi_{J,I}}{2}\right]\frac{1}{2}\left[\left(\frac{X}{m}\right)_{J,I} + \left(\frac{X}{m}\right)_{J-1,I}\right]}{2\Delta x}$$

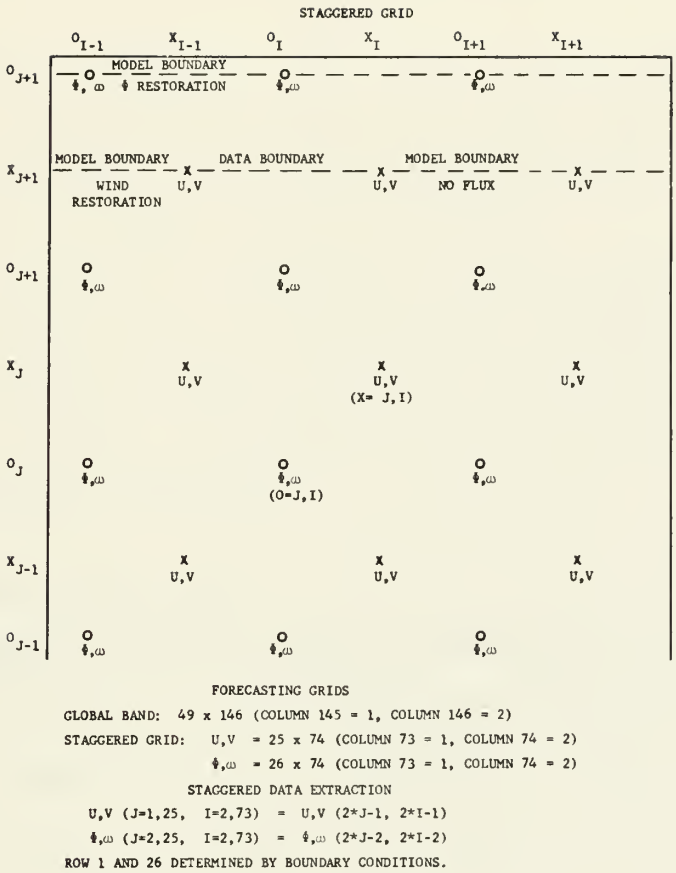

FORECASTING GRIDS

GLOBAL BAND: 49 x 146 (COLUMN 145 = 1, COLUMN 146 = 2)

STAGGERED GRID: U,V = 25 x 74 (COLUMN 73 = 1, COLUMN 74 = 2)

Φ,ω = 26 x 74 (COLUMN 73 = 1, COLUMN 74 = 2)

STAGGERED DATA EXTRACTION

U,V (J=1,25, I=2,73) = U,V (2*J-1, 2*I-1)

Φ,ω (J=2,25, I=2,73) = Φ,ω (2*J-2, 2*I-2)

ROW 1 AND 26 DETERMINED BY BOUNDARY CONDITIONS.

Fig. 1. Staggered grid description

$$- \left[\frac{\phi_{J,I} + \phi_{J,I-1}}{2}\right] \quad \frac{1}{2}\left[\left(\frac{X}{m}\right)_{J,I-1} + \left(\frac{X}{m}\right)_{J-1,I-1}\right]$$
$$2\Delta x$$

The vertical motion used in vertical advection of wind speed is obtained by averaging the four nearest diagonal values of ω.

As in the full grid, this form of finite differencing averages parameters over only two points but results in differencing over two full grid lengths.

Vertical motion is computed from the continuity equation using winds that are obtained by averaging predicted winds over two grid increments located diagonally from the vertical motion gridpoint.

D. BOUNDARY CONDITIONS

The computationally stable integration of the primitive equations requires a set of boundary conditions that are consistent with the finite difference scheme.

Flux through the top of the domain is eliminated by setting $\omega = 0$ at 100 mb.

Two sets of horizontal boundary conditions were tested in the prediction model:

1. No-flux boundaries

Elsberry and Harrison (1971) discuss the boundary conditions that were applicable to the basic ten-level model and which are used in one version of the barotropic model. In the full grid, no flux of mass or energy is allowed at the northern boundary by setting:

$$V_{J+1} = - \frac{m_{J+1}}{m_J} V_J \ , \ U_{J+1} = U_J \ , \ \phi_{J+1} = \phi_J$$

where J+1 is the northern-most row in the grid. The southern boundary is treated in a similar manner. These boundary conditions result in the model boundary being a fictitious grid row between the two outer rows of input data across which there is no flux of mass or energy. East-west boundary conditions are not needed since the global band is continuous.

The u boundary conditions on the staggered grid are similar to those on the full grid. In order to conserve kinetic energy on the staggered grid $\phi_{J+1} = \phi_J$ where J+1 is the northern-most row of the staggered geopotential values. To satisfy the no-flux criterion, the outer row of v component wind must be identically zero. This specification of boundary conditions results in the model boundary being coincident with the outer-most row of staggered grid wind components.

2. Restoration boundaries

Kesel and Winninghoff (1970) describe a constant flux, restoration boundary technique. This technique is used with initial data from the nonlinear balance equation which has consistent boundary conditions, and balancing produced by a numerical variational analysis scheme. Both of these techniques are later described in detail. The restoration technique involves restoring the newly predicted values near the boundaries toward their value at the previous

time step with a specified restoration coefficient. In the full grid prediction, these coefficients are a linear variation of 1.0, 0.8, 0.6, 0.4, 0.2, 0.0. This results in a persistence forecast on the outer boundary, pure dynamical forecast six rows in and a linear combination between. Note that the data boundary is the model boundary. In the staggered grid a similar approach is used with coefficients of 1.0, 0.6667, 0.333, 0.0. In the staggered grid, a fictitious geopotential value is needed one grid length outside the boundary of the available data so a linear extrapolation on the input data geopotential gradient is used:

$$\phi_{J+2,I} = 2\,\phi_{J+1} - \phi_{J}$$

This results in the model geopotential boundary being one row outside the input data boundary and the model wind boundary coinciding with the data boundary.

III. DATA DESCRIPTION

First test experiments with the prognostic and diagnostic models used a climatological input produced by Jenne (1969) of the National Center for Atmospheric Research. In particular, these experiments used 300 mb January climatology for the area of the global band. Although this data lacks the small-scale features which are important in day-to-day forecasting, the strong interaction between the tropics and the middle latitudes through the subtropical jet is present. In addition, boundary condition effects and development of near-equatorial circulations can be tested. The 300 mb level was chosen so that comparable later experiments using real data would allow a maximum of actual observations.

The real data utilized in later experiments are from the Fleet Numerical Weather Central global band analysis developed by Grayson (1971). This analysis covers the entire global band from 60N to 41S. The grid dimensions are 49 X 144 on a Mercator secant projection map true at 22.5° latitude. The mesh length is 2.5° longitude (=150 n.mi.) at the equator and reducing to 75 n.mi. at 60N. This grid size has the capability of depicting relatively small scale synoptic events, provided the observations are sufficiently dense. Grayson (1971) used a modified version of the successive approximations technique to analyze sea

level pressure and surface wind. This approach has subsequently been extended to the analysis of seven levels of upper level winds, but it should be noted that no vertical consistency check is applied. In an attempt to accommodate the large variation of data coverage and the various scales of motion in the wind analysis, the area influenced by each observation, in addition to being dependent on the scan number, is dependent upon the reported wind direction (if greater than 13 knots). This approach was suggested by Endlich and Mancuso (1968).

The previous six hour old analysis is used as a first guess field. 450 reports per analysis is a typical number of reports at 300 mb with approximately the following latitudinal distribution:

45N - 60N = 37%

30N - 45N = 33%

15N - 30N = 20%

15S - 15N = 6%

30S - 15S = 2%

41S - 30S = 2%

No upper air geopotential fields are analysed by the global band analysis program. Therefore, a first guess field is produced using a combination of the current FNWC hemispheric analysis north of 27N and climatology south of 17N with a linear combination in between.

Since the real winds and climatological heights along the southern boundary of the global grid are not geostrophi-

cally consistent, the height values are altered along the boundary. Geostrophic gradients appropriate to the analysed v component of the wind are added to the average climatological height along the southern wall. This approach is applied to all diagnostic models except no-flux boundary conditions where it is not applicable.

IV. INITIALIZATION METHODS

A. NONLINEAR BALANCE EQUATION WITH NO-FLUX BOUNDARY CONDITIONS

Elsberry and Harrison (1971) utilized the nonlinear balance equation and applied no-flux boundary conditions to formulate a diagnostic model which matches the no-flux version of the prediction model. The nondivergent part of the wind is obtained from $\zeta = \nabla^2 \psi$ where ζ is the relative vorticity obtained from the observed u and v wind components. No-flux boundary conditions imply that the north and south boundaries are streamlines with no v component wind across them. Conservation of kinetic energy requires that the two outer rows of ϕ at the boundaries be set equal. In order to avoid setting up gravity waves propagating along the boundary, the geopotential along the entire boundary is set equal to the average value. ψ_{south} is set equal to $\psi_{north} - \bar{u}\Delta y$ where $\bar{u}$ is the mean zonal wind component averaged over the grid and Δy is the distance from the north to south boundary. The natural cyclic east-west boundary conditions alleviate the need for artificial boundaries in this direction.

The nondivergent wind is calculated from the relaxed ψ field using $\bar{v} = \bar{k} \times \bar{\nabla}\psi$. No-flux conditions are forced by making v(49,I) = v(48,I) m(49)/m(48) and similarly at the southern wall where m is the map factor. Then, the geo-

potential field is generated by relaxing $\nabla^2\phi$ using the non-linear balance equation:

$$\nabla^2\phi = \bar{\nabla}f \cdot \bar{\nabla}\psi + f\nabla^2\psi + 2J\left(\frac{\partial\psi}{\partial x}\ \frac{\partial\psi}{\partial y}\right)$$

One should note that large deviations in the geopotential from the input geopotential are to be expected due to the zonal averaging of the boundary values.

B. NONLINEAR BALANCE EQUATION WITH RESTORATION BOUNDARY CONDITIONS

Kesel and Winninghoff (1970) describe a restoration technique which eliminates the need for altering the boundary geopotential field and appears to control false reflection of physical and computational modes at the boundary. Wind and height values of the input data are not altered on the north-south boundaries in contrast to the no-flux method. The technique involves restoring after each time step the values of the parameters near the walls toward the value in the previous time step with a specified restoration coefficient. This results in a purely dynamic forecast in the interior, a persistence forecast on the boundary and a combination in-between. The technique results in the boundaries acting as an energy sponge for externally propagating meteorological and gravity waves.

When working with climatological fields for input data, the southern boundary of ψ was determined similar to the no-flux case by using a column average of the zonal wind component. This technique applied to real data, however, pro-

duced unrealistic meridional velocity components along the southern wall due to the large and rapid variations in the east-west direction of the average zonal wind component. To correct this problem, the ψ's calculated as above are averaged. The southern ψ value is set to this value which results in a north-south ψ gradient consistent with the mean zonal wind. Upon this average value at the southern boundary, variations are superimposed to reflect east-west gradients which are consistent with the analysed v components on the southern wall. The remainder of the balancing is identical to the no-flux approach.

C. NUMERICAL VARIATIONAL ANALYSIS

Lewis (1972) has adapted Sasaki's (1958) variational method to obtain dynamically consistent initial fields from input objective operational analyses. The fields are adjusted so they satisfy the equations of motion and minimize the functional:

$$I = \int_x \int_y [\tilde{\alpha}(u-\tilde{u})^2 + \tilde{\alpha}(v-\tilde{v})^2 + \tilde{\beta}(Z-\tilde{Z})^2 + \alpha(\frac{\partial u}{\partial t})^2 + \alpha(\frac{\partial v}{\partial t})^2]\partial s \quad (9)$$

with $\tilde{u}$, $\tilde{v}$, $\tilde{z}$ being the input analysis. $\tilde{\alpha}$, $\tilde{\beta}$ are weighting functions specified beforehand which can be varied in response to the density and reliability of the input observations and which determine how closely the desired fields u, v, and z fit the input analysis. The dynamic weight α is a similar function which controls the horizontal acceleration (calculated from the momentum equations given below) and directly couples the wind and height information via the

assumed dynamical relations.

$$\frac{\partial u}{\partial t} = - g\frac{\partial Z}{\partial x} - \bar{\bar{v}} \cdot \bar{\nabla} u + fv \qquad \frac{\partial v}{\partial t} = - g\frac{\partial Z}{\partial y} - \bar{\bar{v}} \cdot \bar{\nabla} v - fu$$

The use of these equations as dynamical constraints require the simultaneous solution of the three equations for u, v, and z (so-called Euler equations). To simplify the Euler equations, the inertial terms in the dynamical constraints are modified:

$$\frac{\partial u}{\partial t} = - g\frac{\partial Z}{\partial x} - \tilde{\bar{v}} \cdot \bar{\nabla} \tilde{u} + fv \qquad \frac{\partial v}{\partial t} = - g\frac{\partial Z}{\partial y} - \tilde{\bar{v}} \cdot \tilde{\nabla} \tilde{v} - fu$$

As in the restoration balancing, the climatological southern height values are averaged and altered to make them geostrophically consistent with the v component winds before the NVA analysis is made on the fields.

V. DIAGNOSTIC RESULTS

Diagnostic experiments were aimed at three objectives: compare NVA results with various forms of the nonlinear balance equation; determine NVA weighting constants which most advantageously initialize the prediction model; and test various methods of limiting the divergence in the NVA output.

The first objective was to compare the results from the variational analysis approach against those using the nonlinear balance equation with no-flux and restoration boundary conditions. One should first note the basic difference in solution approach between the two methods. The nonlinear balance alters the geopotential field based on the nondivergent wind input from the streamfunction solution, while the variational analysis simultaneously alters both the winds and geopotential.

Area average wind changes listed in the tables, and wind changes analysed in the charts to follow are obtained by subtracting the input field from the balanced field. Therefore, a positive value means an increase of westerly winds in the u component and an increase in southerly winds in the v component. Area average modulus change is the average of the absolute value of the individual wind changes which gives a measure of the magnitude of the average change at each grid point. The values given are an

average of the u and v component changes which were found to have similar values. The RMS change is the square root of the average of the squares of the balancing changes. RMS u and v components are averaged since similar values were obtained.

Fig. 2 shows a typical v wind component input to the objective analysis programs. Fig. 3 shows the v component changes produced by the nonlinear balance solution with restoration boundary conditions. The nonlinear balance approach tends to reduce the absolute magnitude of the wind maxima in both the u and v component wind with the centers of maximum change being of nearly equal magnitude. This wind change represents the divergent component of the wind. As shown in Table 1, the modulus and root-mean-square change in the no-flux approach are larger than in the restoration approach due to the crude boundary approximations. The non-realistic boundary conditions in the no-flux approach only produce significant differences from the restoration boundaries within about five rows of the boundary. The wind speed changes produced by the variational analysis approach, as displayed in Fig. 4, show smaller magnitudes in a larger scale pattern. Generally, the tendency is to reduce the wind maxima and increase the intervening wind minima. Table 1 shows an average modulus wind change of 0.60 m/sec in the pure NVA analysis as compared to a modulus change approximately four times as large for the nonlinear balance method.

Fig. 2. 300 mb Global band v component wind analysis from 60E to 150W for 08/1200Z January 1972. Units = m/sec.

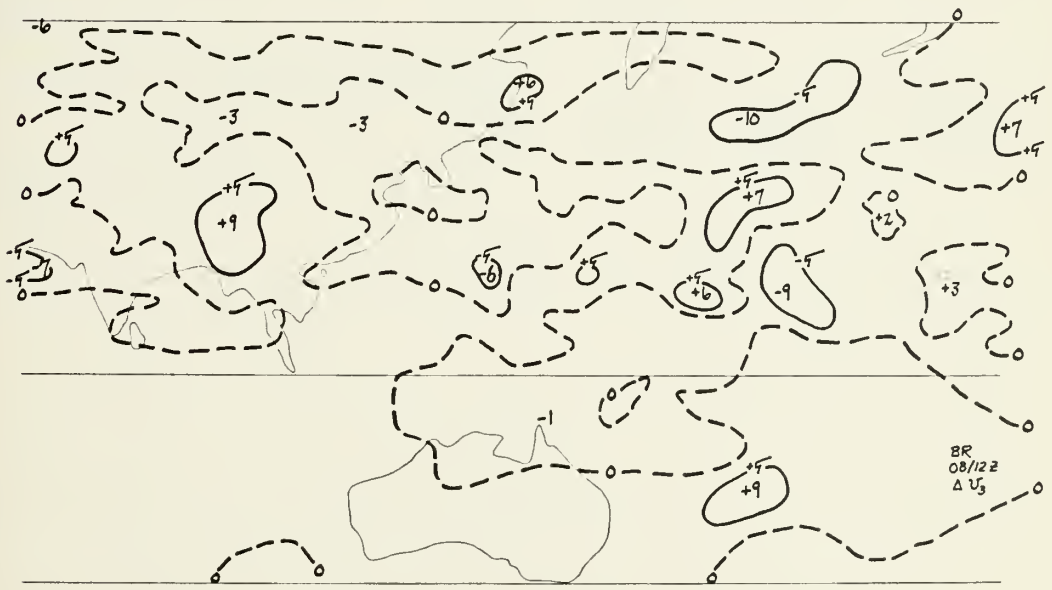

Fig. 3. V component wind speed changes resulting from non-linear balance solution with restoration boundary conditions. Positive (+) value indicates increase in southerly wind speed. Units = m/sec.

TABLE 1

METHODS OF BALANCING

Balancing Type	Area Average Wind Change (m/sec)	Area Average Modulus Wind Change (m/sec)	RMS Wind Change (m/sec)	Area Average Height Change (m)	Area Average Modulus Height Change (m)	RMS Height Change (m)
I. Resulting Field Nondivergent						
NVA (1,7,25) Made Nondivergent	u=.50 v=.27	1.81	2.61	-22.0	31.0	37.0
No-flux Balance Equation	u=-.26 v= .23	2.84	4.12	96.0	131.0	175.2
Restoration Balance Equation	u=-.03 v= .24	1.89	2.87	106.7	131.0	174.4
II. Resulting Field Divergent						
NVA (1,7,25)	u= .52 v= .025	.60	1.10	-22.0	31.0	37.0

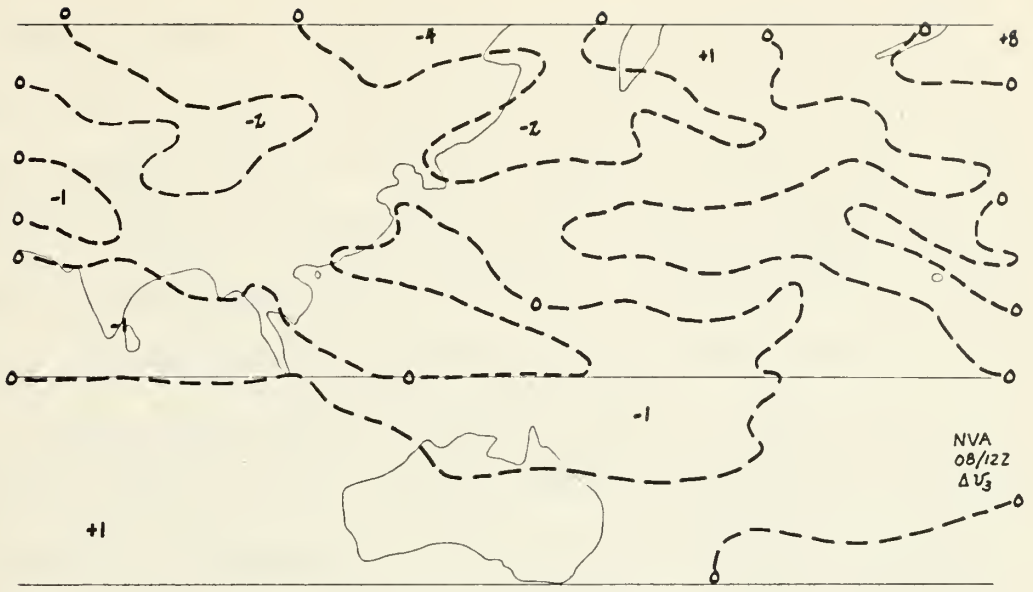

Fig. 4. V component wind speed changes resulting from NVA initialization program (1,7,25). Positive (+) value indicates increase in southerly wind speed. Units = m/sec.

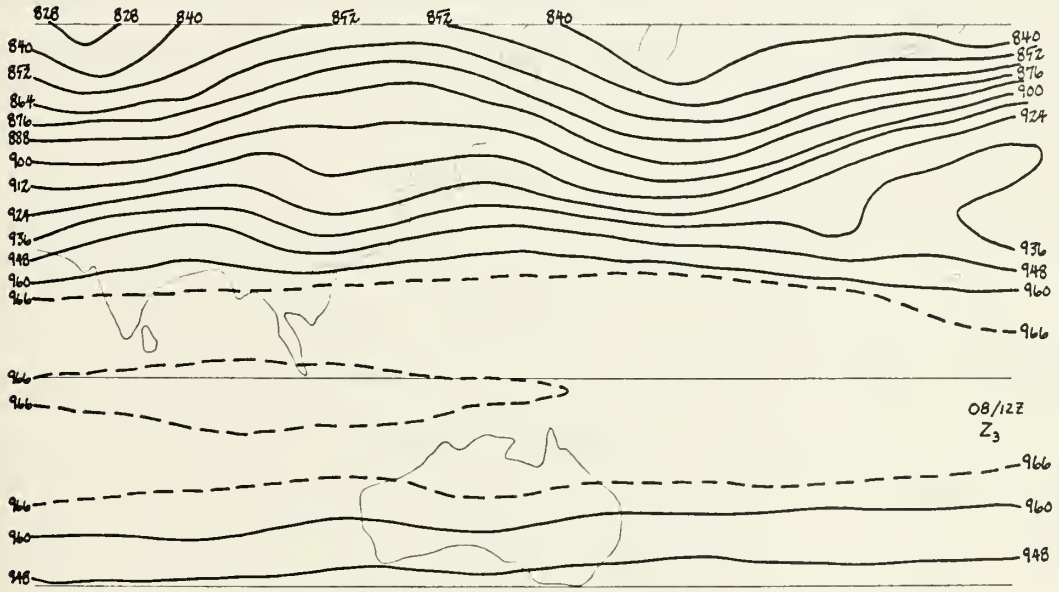

Fig. 5. 300 mb Global band height field from 60E to 150W for 08/1200Z January 1972. Units = decameters.

Fig. 5 shows the 08/1200Z January 1972 global band height field used in these experiments. In evaluating height changes produced by the various methods, one must remember that the geopotential field was obtained from the derived nondivergent wind analysis. In addition, approximately two-thirds of the height field, that south of 17N, is a climatology field. Keeping this in mind, one can see from Table 1 that the NVA analysis alters the heights only about one-quarter as much as the nonlinear balance approach. In the region with real height data, the NVA analysis tends to fill troughs and reduce ridge heights in order to achieve balance. These changes appear to be displaced toward the downwind side of the synoptic feature in the mid-latitudes. The scarcity of data in the southern hemisphere tends to produce isolated wind maxima and the NVA introduces height gradients to partially balance these winds. Fig. 6 shows that the NVA height changes necessary to generate gradients consistent with the winds are both positive and negative, and the changes are similar in scale to the wind maxima themselves. By contrast, the changes in the two cases using the nonlinear balance equation approach are on a much larger scale as shown for the no-flux case in Fig. 7. The patterns are on the order of the long waves that are present, and the changes tend to deepen the troughs by building a ridge downwind of the trough axis. Unlike the NVA results, all height changes are positive in the northern hemisphere and are about four times

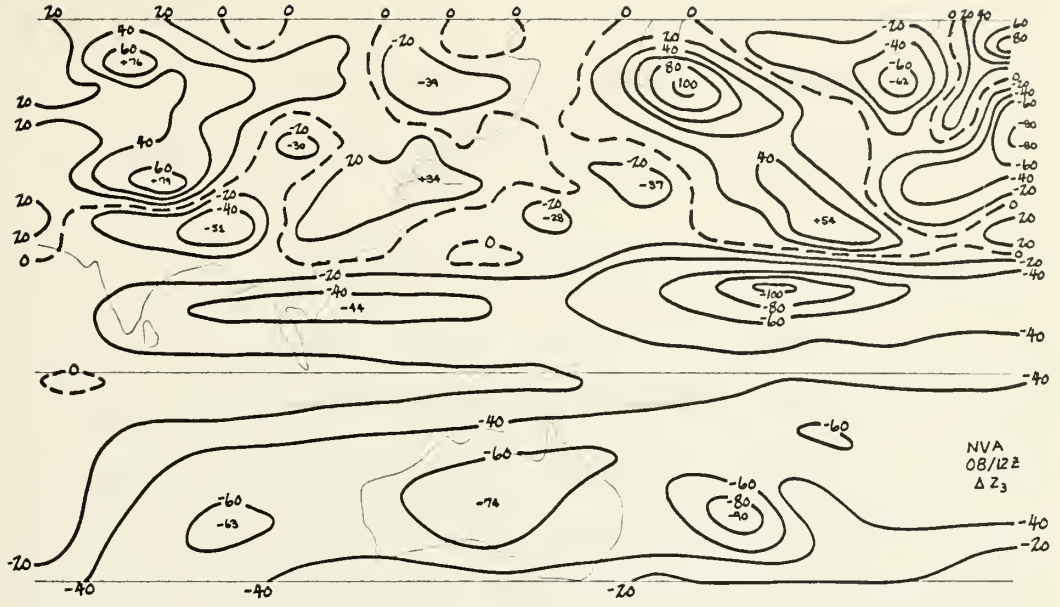

Fig. 6. Height changes resulting from NVA initialization program (1,7,25). Units = m.

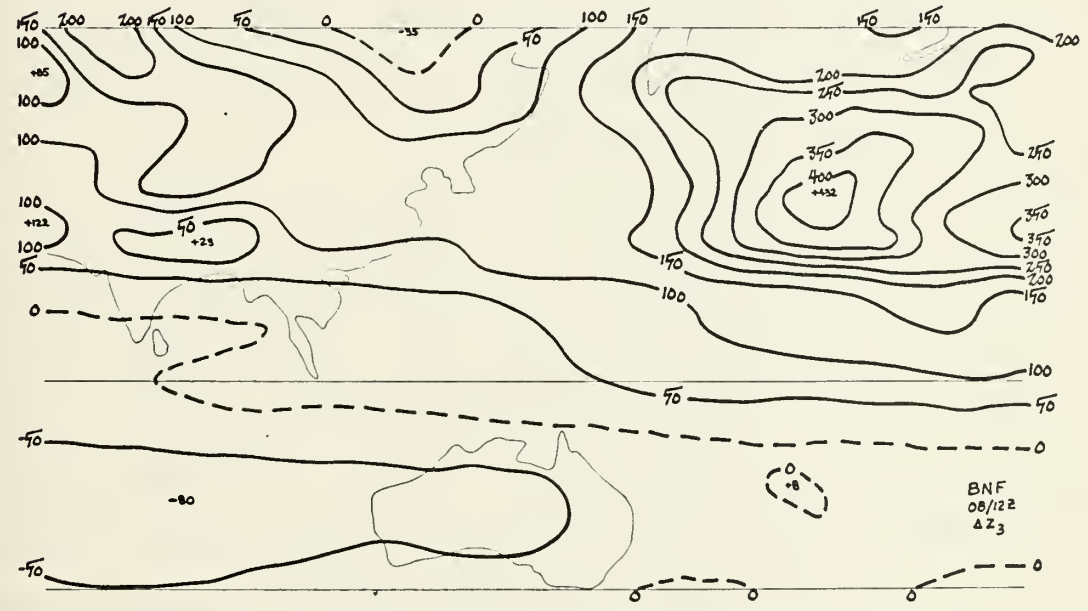

Fig. 7. Height changes resulting from nonlinear balance solution with no-flux boundary conditions. Units = m.

as large as those in the NVA. Area average changes are slightly larger in the no-flux boundary condition than in the restoration case, since the boundary heights are constant.

Early development experiments made use of climatological data as mentioned before. One would expect these fields to be composed of long wave features with none of the short wave systems apparent in daily analyses. This is evident in the wind and height changes necessary to balance the real data fields. The wind changes due to initialization of the climatological data are one-fourth to one-half of those for real data.

The second objective of the diagnostic experiments was to develop weighting values for the variational analysis scheme which produced fields with sufficient balancing to successfully initialize the prognostic program. Table 2 shows the results of this experimentation. Since only a wind analysis is available in the tropics, the NVA analysis should be forced toward the wind values with little weight on the height values. The dynamical constraint should be large enough to assure compatibility as an initial state for the prediction model. One must pay the price of additional computer time if the analysis is to be forced toward exact balance, or small deviations from the input wind fields, as shown in Fig. 8. An arbitrary root-mean-square deviation in the wind field of 1.0 m/sec was set as a desirable limit on changes allowed from the input value.

TABLE 2

VARIATIONAL ANALYSIS WEIGHTS

$\tilde{\alpha}$ = winds

$\tilde{\beta}$ = geopotential

α = dynamics

Balancing Weights $\tilde{\beta}$, $\tilde{\alpha}$, α	Area Average Wind Change (m/sec)	Area Average Modulus Wind Change (m/sec)	RMS Wind Change (m/sec)	Area Average Height Change (m)	Area Average Modulus Height Change (m)	RMS Height Change (m)
1,1$\frac{1}{2}$,25	u=1.43 v= .13	1.40	2.47	-16.5	29.0	35.6
1,7,25	u= .52 v= .025	.63	1.10	-22.1	31.0	37.0
1,16,25	u= .26 v= .03	.33	.60	-25.2	34.8	42.7
1,25,25	u= .17 v= .02	.22	.41	-26.5	35.6	43.7

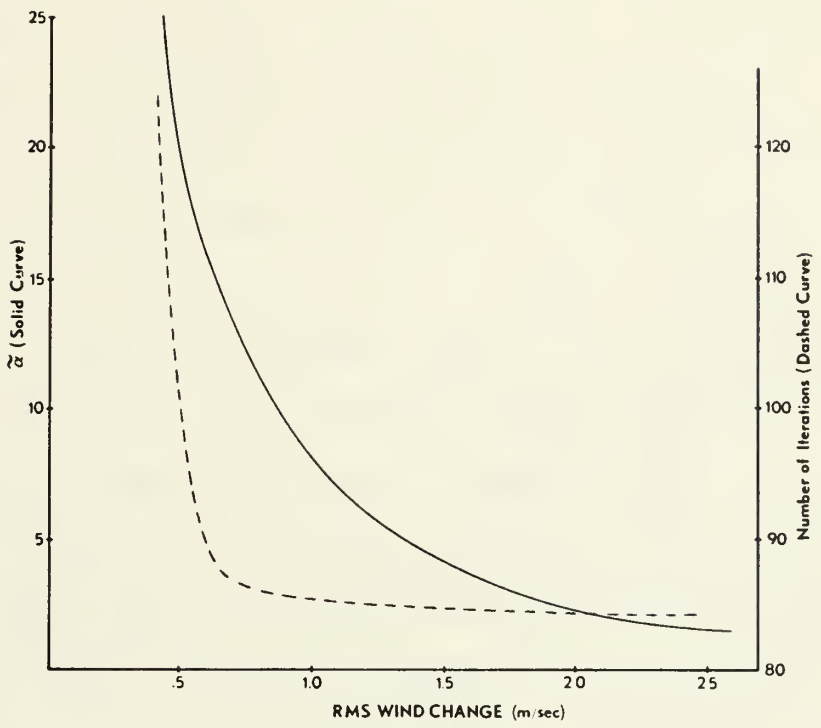

Fig. 8. NVA wind weighting factor (solid), and number of iterations required for convergence (dashed) for a RMS wind difference between final and initial fields. The values of pressure and dynamical weighting factors are held fixed.

This resulted in an $\tilde{\alpha}$ value of approximately 7.0 when combined with $\tilde{\beta}$ = 1.0 and α = 25.0 where $\tilde{\beta}$ limits height changes, α specifies the degree of horizontal acceleration in the wind field and $\tilde{\alpha}$ limits the wind changes as specified in Eqn. 9. One should note that limiting the wind deviations to very small changes causes a rapid increase in the number of iterations required for convergence. Specifying the coefficients of 1,7,25 required approximately 23 seconds of computer time for each iteration of the unconverged points. This results in a total run time of about 32 minutes which is extremely long for an operational analysis. In contrast, the nonlinear balance approach requires approximately eight minutes of computer time.

It was discovered in the experiments with climatological data that the wind fields resulting from the variational analysis program produced excessive two-gridlength gravity waves and excessive vertical motions. Eventually, this noise led to computational instability. The NVA procedure satisfies the dynamical constraints on the fields by limiting the magnitude of horizontal accelerations, which are obtained from the wind tendency equations. There is no direct control on the amount of divergence allowed. Therefore, the third objective of the initialization experiments was to evaluate various methods of limiting divergence in the NVA output field. Two alternatives existed; make the input wind fields to the NVA analysis nondivergent and produce a divergent output; or make the output of the NVA program non-

divergent by using only the nondivergent component. However this postadjustment of the wind will create some inconsistency with the height field that was produced by the NVA scheme.

A FNWC subroutine, which uses version III of the method described by Hawkins and Rosenthal (1965), was used to compute the nondivergent wind. It should be noted that this approach does not retain the original u and v winds on the boundary as boundary conditions. Nevertheless, changes are minimal on the boundaries.

Table 3 shows the results of these experiments. The patterns of wind changes necessary to make the fields nondivergent show patterns similar to those of the nonlinear balance equation, however, on a smaller scale, as shown in Fig. 9. The individual wind maxima are altered similar to the scale of the NVA changes. One can see that the NVA program changes the winds approximately the same amount whether the input is divergent or nondivergent; however, the height changes necessary with the nondivergent input are larger. The modulus and root-mean-square wind changes necessary to make the fields nondivergent are about two and one-half times larger than changes in the NVA analysis. Nevertheless, the total change involved in both methods are very nearly equal. It should be pointed out that a property of a nondivergent field is that a cyclic row average of the v component wind around the global band equals zero. This implies no net mass transport in the meridional direction.

TABLE 3

VARIATIONAL ANALYSIS METHODS

Method	Area Average Wind Change (m/sec)	Area Average Modulus Wind Change (m/sec)	RMS Wind Change (m/sec)	Area Average Height Change (m)	Area Average Modulus Height Change (m)	RMS Height Change (m)
Method 1						
a. Divergent Input Made Nondivergent	u=.25 v=.27	1.75	2.54	None	None	None
b. Nondivergent Input To NVA (1,7,25)	u=.50 v=-.02	.59	1.00	-31.4	40.2	50.8
Total Change	u=.75 v=.25	1.80	2.54	-31.4	40.2	50.8
* *						
Method 2						
a. Divergent Input To NVA (1,7,25)	u=.52 v=.025	.60	1.10	-22.0	31.0	37.0
b. NVA (1,7,25) Output Made Nondivergent	u=-.02 v=.25	1.67	2.44	None	None	None
Total Change	u=.50 v=.27	1.81	2.61	-22.0	31.0	37.0

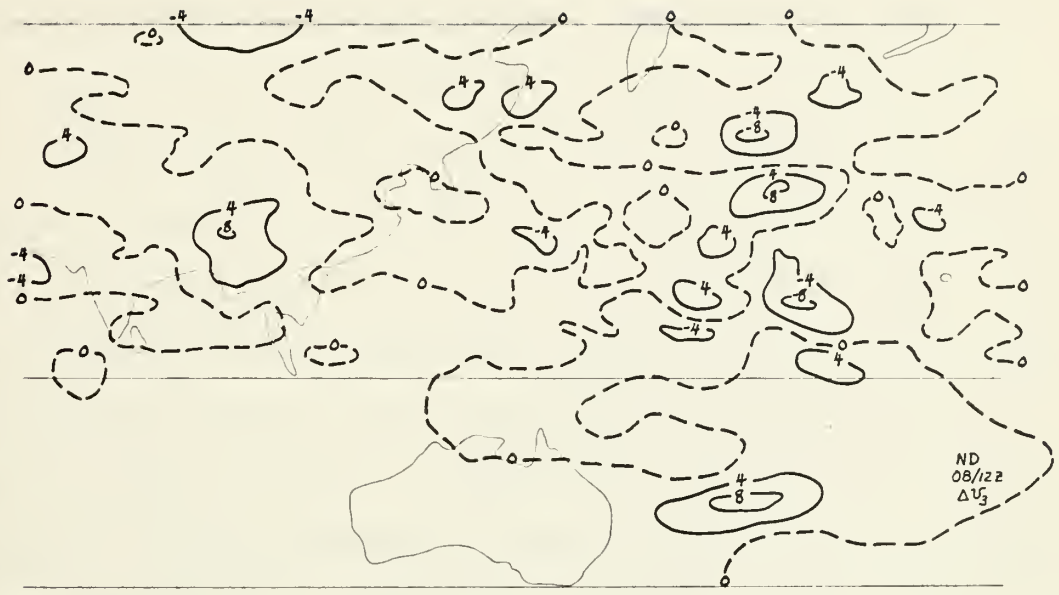

Fig. 9. V component wind speed changes resulting from nondivergent subroutine. Positive (+) value indicates increase in southerly wind speed. Units = m/sec.

VI. PREDICTION RESULTS

A. BOUNDARY CONDITIONS

Boundary conditions on a global band pose problems different than those in a hemispheric model. The global band boundaries are in the mid-latitudes where strong meridional flow causes strong cross-boundary fluxes. A hemispheric model avoids these difficulties, since boundaries are located in the tropics where pressure gradients are relatively small and large scale waves are not commonly present. The major problem in the prediction models caused by the large cross-boundary flow is the generation of gravity waves at and near the boundaries. These waves contaminate the prediction of the meteorological waves and may lead to computational instability. Prediction on the full grid with no-flux boundary conditions produce only small amplitude gravity waves. Restoration boundary conditions with compatible nonlinear balance equation input to the prediction model produce strong two-gridlength gravity waves, which require filtering to obtain a stable 24-hour forecast. This filtering is accomplished using a scheme devised by Shapiro (1971) in which the variable's value at J,I is altered by 1/8 $(S_{J+1,I} + S_{J-1,I} + S_{J,I+1} + S_{J,I-1} - 4\,S_{J,I})$ where S is a general variable. In order to obtain a 24-hour forecast, it was necessary to apply the filter once every four hours. Figs. 10 and 11 show the gravity wave effect in the RMS ϕ

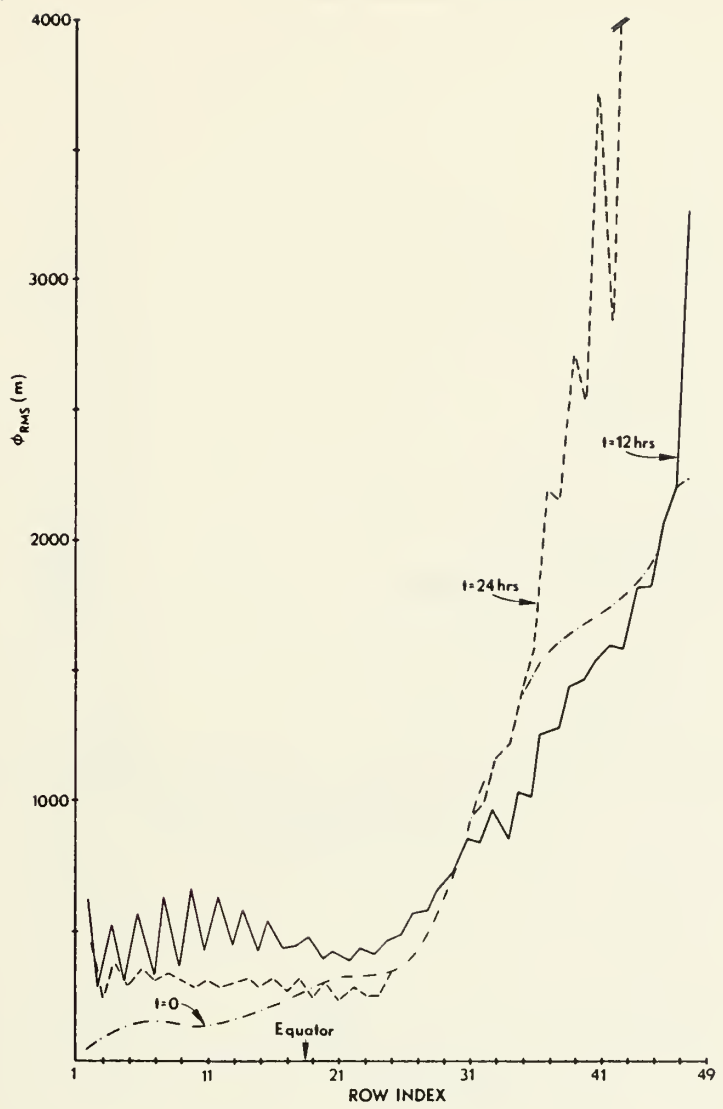

Fig. 10. ϕ_{RMS} vs. Grid Row for full grid restoration prediction. Units = m.

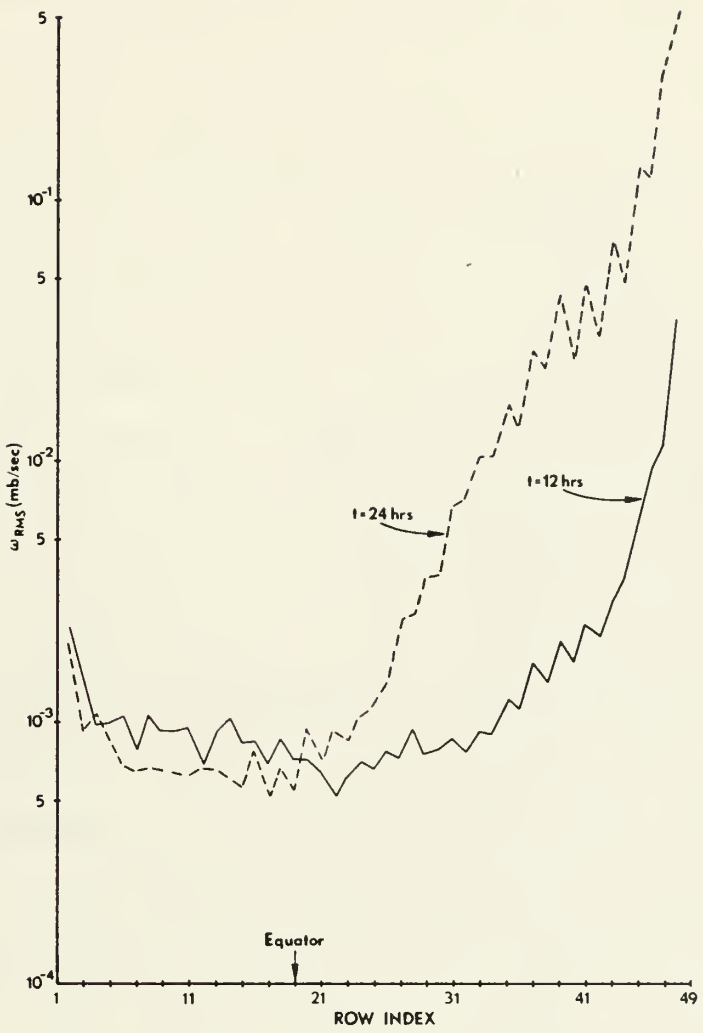

Fig. 11. ω_{RMS} vs. Grid Row for full grid restoration prediction. Units = mb/sec.

and RMS ω values respectively. The 2-d nature of the gravity waves is evident in both fields. The cross-boundary flow and resulting gravity waves produce much larger RMS ϕ and ω values near the northern wall which increases in amplitude with time. NVA input to the full prediction model resulted in the most severe 2-d waves, as might be expected since the dynamic constraint is not as strong as in the nonlinear balance approach. It was necessary to apply the filter twice at four-hour intervals to produce a 24-hour forecast. The staggered grid predictions did not require any filtering to produce a stable 24-hour forecast. RMS ϕ and RMS ω for the staggered grid restoration prediction, shown in Figs. 12 and 13, are much better behaved than in the full grid prediction. At t=0, the ω curve in Fig. 13 arises from extracting alternate u and v component winds from the balanced solution obtained on the full grid. Therefore, the staggered field contains divergence while the full grid field is nondivergent and contains no vertical motion at t=0. The vertical motions in the staggered prediction maintain the same size ω as time increases. The amplitude of the two-gridlength waves is not as great and values at the northern boundary do not increase in amplitude as rapidly with time as in the full grid prediction models. This is to be expected since the finite differencing involves calculations over two gridlengths of the full grid and results in the use of points which have a similar phase angle with respect to the 2-d waves.

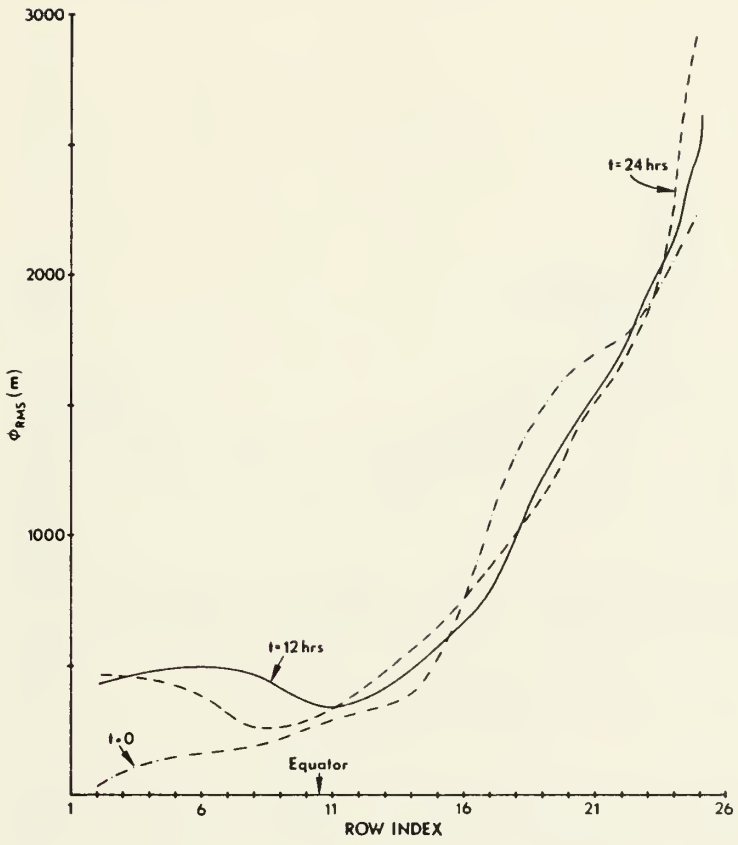

Fig. 12. ϕ_{RMS} vs. Grid Row for staggered grid restoration prediction. Units = m.

Fig. 13. ω_{RMS} vs. Grid Row for staggered grid restoration prediction. Units = mb/sec.

B. PREDICTION VERIFICATION METHODS

The output fields were smoothed with a filter which altered the parameter value at J,I by 1/8 ($S_{J+1,I}+S_{J-1,I}+S_{J,I+1}+S_{J,I-1}-4\ S_{J,I}$). Verification of the prognosis was based on these filtered fields. Also, to avoid unrealistic fields produced by the restoration process near the boundaries, and fictitious boundary specification in the objective analysis, verification statistics were only computed in the interior region where a true dynamical forecast was computed. This excluded the outer six rows in the full grid prediction and the outer four rows in the staggered grid. Verification criteria for predictive models are numerous and by no means obvious. The area average modulus wind component differences and the RMS differences were chosen since accuracy in the wind analysis is more desirable in the tropics than are good height values. A single numerical value which was used to combine the various measures of forecast ability was defined as in the following formula:

$$\text{Forecast Value} = (|u|_{\text{Persist}} - |u|_{\text{Verif}}) + (|v|_{\text{Persist}} - |v|_{\text{Verif}}) + (u_{\substack{\text{RMS}\\\text{Persist}}} - u_{\substack{\text{RMS}\\\text{Verif}}}) + (v_{\substack{\text{RMS}\\\text{Persist}}} - v_{\substack{\text{RMS}\\\text{Verif}}}) \qquad (10)$$

where $|u|$ = area average modulus error

u_{RMS} = root mean square error

Persistence forecast error is defined as the comparable

balanced field at t_o+24 hours minus the comparable balanced field at t_o. Lavoie and Wiederanders (1968) have pointed out that in the tropics a persistence forecast plus a variable amount of climatology is still difficult to beat with any objective prediction technique.

Typical magnitude persistence forecast error values are shown in Table 4.

Verifying forecast error is equal to the predicted values at t_o+24 hours minus the verifying balanced field at t_o+24 hours. Therefore, if the forecast value is positive, the verification is better than persistence with increasing magnitudes denoting better verification skill.

A negative value implies less skill than a persistence forecast. Less emphasis was placed on height verification since these fields are derived rather than analysed. However, one measure of prediction accuracy is the ratio of RMS persistence height change to the RMS verification height error. Numbers less than one imply a persistence forecast is more accurate. Values of this ratio greater than one imply forecast skill compared to persistence. These values are shown in Tables 5 and 6 in parentheses.

The number of passes through the predicted fields with the smoother had a definite effect on the verification statistics. A typical example with the forecasts with NVA input is shown in Table 4. The modulus and RMS verification values for the v component are better than persistence, regardless of the number of filter passes. Successive

TABLE 4

VERIFICATION STATISTICS AS FUNCTION OF FILTER PASSES

Forecast: Non-divergent NVA input (1,7,25)

Number of Passes	Area Average Modulus u Component Wind Difference (m/sec)	Area Average Modulus v Component Wind Difference (m/sec)	RMS u Component Wind Difference (m/sec)	RMS v Component Wind Difference (m/sec)	Area Average Modulus Height Difference (m)	RMS Height Difference (m)
Persistence	4.19	5.45	7.01	10.25	31.35	63.40
None	4.82	4.35	7.05	7.25	51.05	71.66
1	4.46	4.15	6.48	6.94	49.29	68.89
2	4.32	4.07	6.24	6.78	48.57	67.73
3	4.27	4.04	6.13	6.70	48.18	67.09
4	4.27	4.02	6.10	6.65	47.97	66.70
5	4.30	4.03	6.12	6.63	47.92	66.60
6	4.34	4.04	6.16	6.64	48.02	66.66
7	4.40	4.04	6.23	6.64	48.15	66.75

filtering up to four or five times improves the verification values. However, beyond five filterings, the verification values begin to decline. The u wind component verification is different, however. Area average modulus u component differences remain higher than persistence values. RMS u component differences with one pass of the filter are smaller than for a persistence forecast and continue to improve up to four or five passes. This can be explained by noting that wind gradients north and south of u component wind maximum are much larger than the gradients around v component wind maximum (see Figs. 14 and 16). Therefore, a slight displacement of the predicted maximum north or south of the actual position leads to larger errors than are produced in the v component by east-west phase errors. Even though filtering reduces the actual jet core speed, the diffusion of the maximum due to filtering results in a better verification value.

Figs. 14 through 19 show the fields used for NVA prognosis verification, and the prognosis error fields for the v component, u component and height fields respectively. All fields, especially the v component and height field show that horizontal advection of most of the synoptic features was too rapid. Predicted positions and intensity of the major synoptic features are shown by the stars and values in parentheses on the verification charts. One can see that the analysed error values are predominantly a function of position, and not intensity or addition/deletion

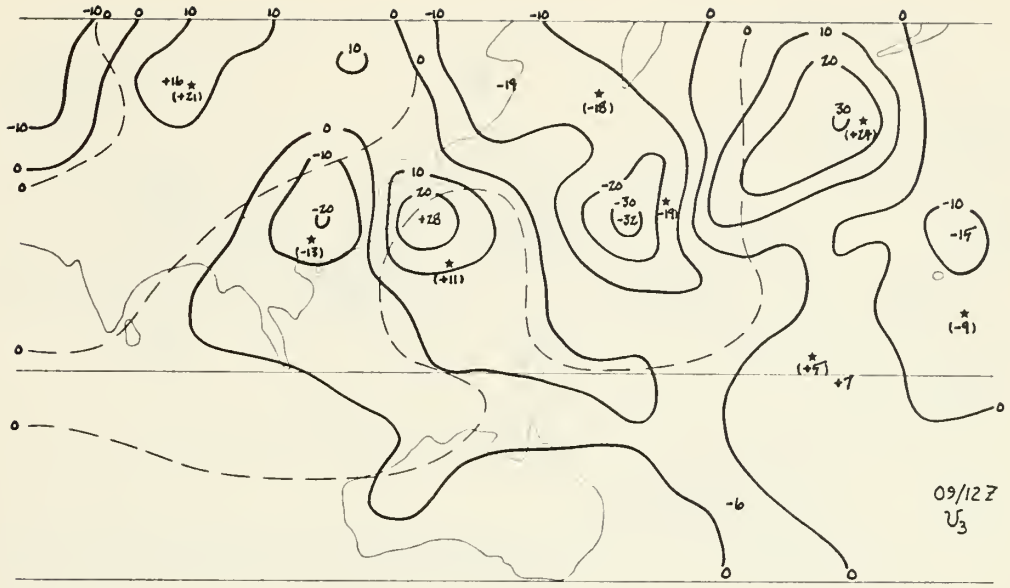

Fig. 14. 300 mb NVA balanced v component wind verification analysis from 60E to 150W for 09/1200Z January 1972. Star denotes prognosis wind maxima location with intensity in parenthesis. Units = m/sec.

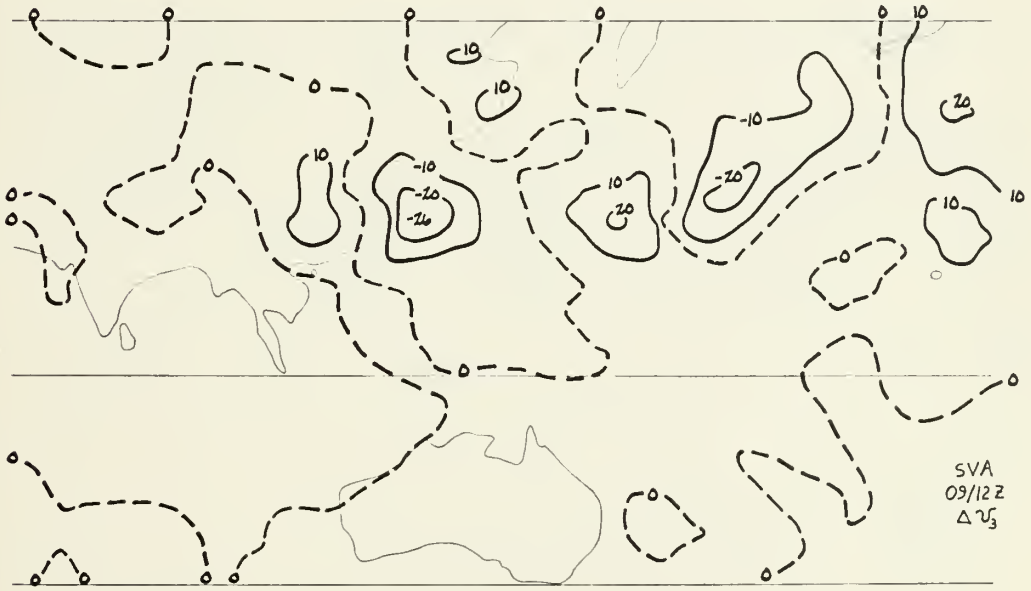

Fig. 15. Nondivergent input NVA prediction verification error of v component wind. Positive (+) value indicates too strong southerly wind. Units = m/sec.

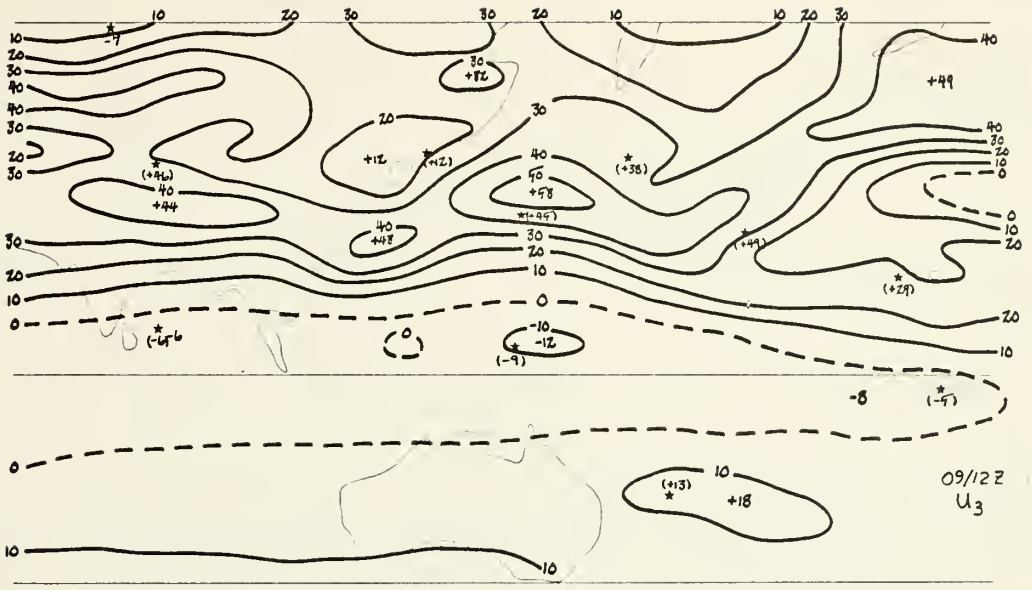

Fig. 16. 300 mb NVA balanced u component wind verification analysis from 60E to 150W for 09/1200Z January 1972. Star denotes prognosis wind maxima location with intensity in parenthesis. Units = m/sec.

Fig. 17. Nondivergent input NVA prediction verification error of u component wind. Positive (+) value indicates too strong westerly wind. Units = m/sec.

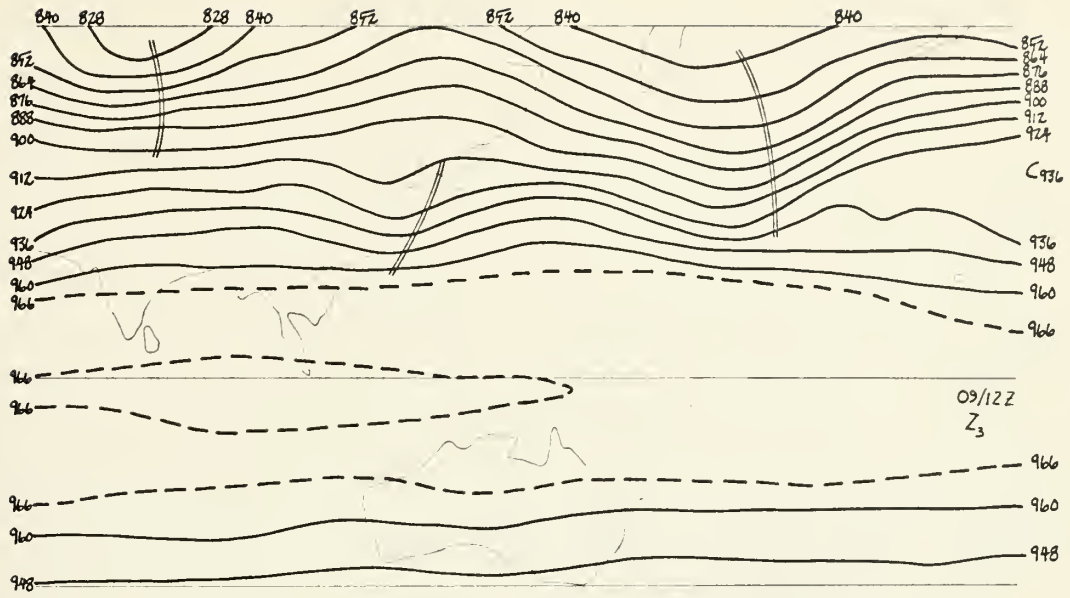

Fig. 18. 300 mb NVA balanced height verification field from 60E to 150W for 09/1200Z January 1972. Trough symbol denotes prognosis trough position. Units = decameters.

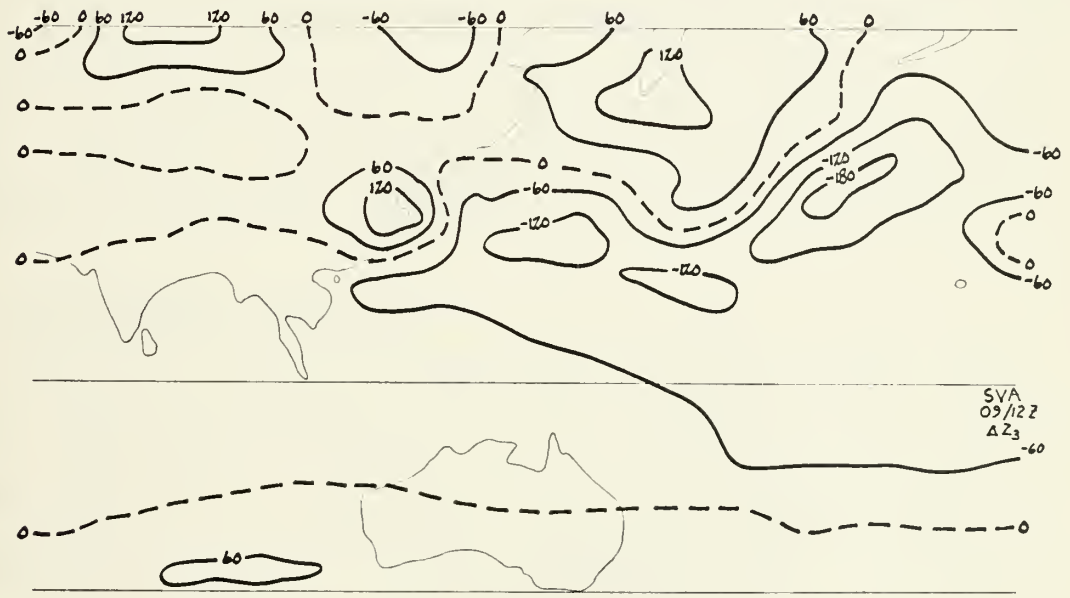

Fig. 19. Nondivergent input NVA prediction verification error of height field. Units = m.

of systems. A typical example is the short wave trough southwest of Korea. The prediction model overpredicts the trough movement (See Fig. 18) with a resulting positive height error pattern west of the predicted trough position and a negative center east of the trough (see Fig. 19). The model moves both of the v component maxima associated with the trough too far south as shown in Fig. 14. This position error contributes about one-half of the value of the verification error analysis shown in Fig. 15. The remainder of the error is due to an underestimate of the magnitude of the v component maxima, which seems to be true of the majority of the centers. The u component wind minima associated with the trough is forecast to move more rapidly eastward than the verifying position shown in Fig. 16. This is depicted in Fig. 17 as a negative error center east of Korea and a positive center west of Korea. Unlike the v component winds, the prediction appears to retain u component magnitudes comparable with the verification.

C. RESTORATION TECHNIQUES

Results of the experiments with climatological input data had suggested that restoration of both wind fields and the height field at each time step also tended to generate excessive 2-d gravity waves originating from the boundaries. This can be explained as follows: As the wind and height fields in the region of outflow try to adjust to the fixed boundary values, the restoration coefficient allows only

partial adjustments. This produces a continual imbalance, which is manifested by gravity waves propagating from this region. The generation of these unwanted gravity waves can be reduced by either restoring the wind values and not the heights, or vice-versa. Slightly smaller amplitude gravity waves were produced, and better verification values were obtained, when u and v component winds were restored with no restoration of the height field. This result is shown in Table 5A for both the full and staggered grid results where Forecast value is defined as in Eq. 10 and the value in parenthesis is the ratio of RMS height error to a RMS height error from a persistence forecast.

D. DIVERGENCE VALUES OF INPUT NVA FIELDS

As mentioned earlier, a limitation of the divergence in the NVA input to the prediction model appeared to have desirable effects on the elimination of unwanted two-grid-length gravity waves. This might be expected to have an effect on the verification values of the prediction, and is shown in Table 5B. The best verification was obtained using an NVA output made nondivergent input to the prediction (Method 2 in Table 3). Slightly worse results were obtained from NVA input data obtained from a nondivergent input into the NVA program (Method 1 in Table 3). Considerably less skill was achieved using initial data from the NVA program with divergent input (Method 2a in Table 3). In fact, the full grid prediction model blew up before a 24-hour forecast could be obtained. One would expect a wind field which was

TABLE 5

PROGNOSIS VERIFICATION AS A FUNCTION OF
RESTORATION, NVA DIVERGENCE, NVA WEIGHTING

Input	Restore	Forecast Value
A. RESTORATION		
Full Grid		
Restoration	ϕ	2.08 + (.77)
Restoration	u & v	2.13 + (.68)
Staggered Grid		
Restoration	ϕ	2.82 + (.61)
Restoration	All	2.90 + (.65)
Restoration	u & v	3.77 + (.58)
NVA(1,7,25)made nondivergent	ϕ	5.69 + (.91)
NVA(1,7,25)made nondivergent	All	5.80 + (.93)
NVA(1,7,25)made nondivergent	u & v	5.86 + (.95)
B. NVA DIVERGENCE		
Full Grid		
NVA(1,7,25)with nondivergent input	u & v	4.37 + (.69)
NVA(1,7,25)made nondivergent	u & v	4.52 + (.84)
Staggered Grid		
NVA(1,7,25)with nondivergent input	u & v	5.73 + (.96)
NVA(1,7,25)made nondivergent	u & v	5.86 + (.95)
C. NVA WEIGHTING		
Full Grid		
NVA(1,1-1/2,25)	u & v	Computational Instability
NVA(1,7,25)	u & v	Computational Instability
NVA(1,25,25)	u & v	3.30 + (.49)
Staggered Grid		
NVA(1,1-1/2,25)	u & v	3.34 + (.78)
NVA(1,7,25	u & v	3.57 + (.75)
NVA(1,25,25)	u & v	3.91 + (.72)

nondivergent to produce fewer gravity waves than a divergent wind field, and the resulting gravity waves appear to be one factor responsible for degrading the verification results in the divergent NVA input wind fields.

E. EFFECT OF NVA WEIGHTING

A variation of the weighting factors in the NVA analysis could be expected to vary the prognosis verification. A closer specification of the wind changes allowed in the NVA analysis (larger $\tilde{\alpha}$) should produce a better forecast wind field, as described in the diagnostic results section on NVA weighting. Table 5c shows this result for the staggered grid prediction. In the full grid, specifying $\tilde{\alpha}$=25 produced a computationally stable prediction for 24-hours, but using $\tilde{\beta}$ = 7 or 1.5 did not adequately limit the changes in the wind components and the predictions became unstable before 24-hours.

F. STAGGERED VS. NON-STAGGERED GRID

Tables 5 and 6 point out that the staggered grid predictions in all cases produce more accurate forecasts than a full grid with comparable input. It is difficult to determine if this is a result of the removal of the computational mode from the walls by use of the staggered grid or an even more severe overprediction of the movement of systems in the full grid compared to the staggered grid. The excessive amplitude of the 2-d gravity waves evident in the full grid predictions, as compared to the staggered grid, appears to

be the most significant influence.

G. COMPARISON OF INITIALIZATION METHODS

On both the staggered and the nonstaggered grids, the NVA fields made nondivergent input to the prediction had the best verification value. Considerably poorer were the balance restoration and balance no-flux, with the forecasts with restoration being slightly better (see Table 6). Better verification of the NVA input might be expected since the changes necessary in the diagnostic phase of prediction are smaller for winds and much smaller for height than in the nonlinear balance method. This results in individual synoptic features retaining their identity and as a result are forecast more accurately.

TABLE 6

PROGNOSIS VERIFICATION AS A FUNCTION OF INITIALIZATION TYPE

Input	Restore	Forecast Value
Full Grid		
No-Flux		.20 + (.57)
Restoration	u & v	2.13 + (.68)
NVA(1,7,25)made nondivergent	u & v	4.52 + (.84)
Staggered Grid		
No-Flux		3.55 + (.55)
Restoration	u & v	3.77 + (.58)
NVA(1,7,25)made nondivergent	u & v	5.86 + (.95)

VII. CONCLUSIONS AND RECOMMENDATIONS

The staggered grid forecasts produced better verification statistics than the full grid. This is desirable since the barotropic full grid prediction requires approximately 33 minutes of computer time for a 24-hour forecast, while the staggered grid requires only about 10 minutes. This is a considerable saving of time when considering operational requirements.

Restoration near the boundaries of the u and v component winds and no restoration of the height field produced better verification values than restoring all fields or restoring only the height field. This results in a slight additional reduction in computer time.

A nondivergent NVA input to the prediction model produced better verification statistics than either the balance restoration or balance no-flux technique. Nondivergent NVA input also produced better verification statistics than NVA fields which had no constraint on divergence. The smallest amount of adjusting of wind speed from the input fields, offset by rapidly increasing NVA convergence time, produced better verification values. To obtain these NVA fields required running two programs with a combined run time of about thirty-five minutes. Again, this is excessive for an operational product. Three changes are possible to reduce the computation time. First, the NVA program could be

altered to place an additional constraint on the magnitude of the divergence of the resulting fields. This would eliminate the need for running the nondivergence program. Also, further experiments might show that a specified amount of divergence results in a better initial field than no divergence. Also, time might be reduced by altering the values of the NVA coefficients to require less adherence to the input fields, and possibly larger tolerances on the horizontal acceleration. The most significant time saving could be realized by converting the NVA program to operate on a staggered grid. This would allow for a solution considering only one-quarter of the present points. Since iterative processes are inherently more efficient on a smaller grid, the time savings should be well in excess of a factor of four.

Boundary conditions on the Mercator belt still remain a problem. Research by Lieutenant Commander E. Harrison (personal communication) on appropriate boundary conditions for numerical models has suggested a different method of handling the prediction in regions of outflow.

It is to be expected that a barotropic model, which can only advect synoptic features with the wind at one level, should produce errors in displacement; specifically a 300 mb level should overforecast movement. In the real atmosphere the vertical differences in both temperature and momentum advection can make the barotropic approximation a poor one. This would suggest that a baroclinic model would give

significantly better movement forecasts. The staggered grid now makes a three- or four-level model operationally feasible. Initial experiments, on a limited grid used by Harrison (1969) and Steinbruck (1971), have shown that at least a three-level model is desirable. At present, the time step in the staggered prediction models is five minutes. This could be doubled if the advection of the height field in Eq. 5 was finite-differenced over twice the present space increment in the full grid, as is the case for momentum advection, with a staggered grid in the time sense. The use of semi-implicit time differencing in the prediction models would also be a means for increasing the time step. One possible approach is a time-averaging form suggested by Brown (1971).

By using at least three layers, it is possible to parameterize the effect of cumulus convection, which is so important in the tropics. A baroclinic model would also make experiments with tropical cyclones movement and development feasible.

BIBLIOGRAPHY

1. Arakawa, A., 1966: Computational design for long term numerical integration of the equations of fluid motion, Part I. Journal of Computational Physics, 1, 119-143.

2. Brown, J. and Campana, K., 1971: A New Explicit Differencing System for Primitive Equations, Unpublished National Meteorological Center Manuscript.

3. Eliassen, A., 1956: A Procedure for Numerical Integration of the Primitive Equations of the Two-parameter Model of the Atmosphere, Technical Report No. 4, Department of Meteorology, Los Angeles.

4. Elsberry, R. L. and Harrison, E. J., 1970: Some primitive equation model experiments for a limited region of the tropics, Proceedings of the 6th AWS Technical Exchange Conference, U. S. Naval Academy, Technical Report 242.

5. Elsberry, R. L. and Harrison, E. J., 1972: Effects of Parameterization of Latent Heating in a Tropical Prediction Model, to be published in the Journal of Applied Meteorology.

6. Elsberry, R. L. and Harrison, E. J., 1971: Height and kinetic energy oscillations in a limited region prediction model, Monthly Weather Review, 99, 11, 883-888.

7. Endlich, R. M. and Mancuso, R. L., 1968: Objective analysis of environmental conditions associated with severe thunderstorms and tornadoes, Monthly Weather Review, 96, No. 6, 342-350.

8. Grayson, T., 1971: Global Band Sea Level Pressure and Surface Wind Analysis, Fleet Numerical Weather Central, Monterey Report.

9. Haney, R. L., 1971: A Numerical Study of Large Scale Response of an Ocean Circulation to Surface Heat and Momentum Flux, Ph.D. Dissertation, University of California, Los Angeles.

10. Harrison, E. J., 1969: Experiments with a Primitive Equation Model Designed for Tropical Application, M. S. Thesis, Naval Postgraduate School.

11. Hawkins, H. F. and Rosenthal, S. L., 1965: On the computation of stream functions from the wind field, Monthly Weather Review, 93, 4, 245-252.

12. Jenne, R. L., Crutchner, H. L., van Loon, H., Taljaard, J. J., 1969: A Selected Climatology of the Southern Hemisphere: Computer Methods and Data Availability, Technical Note, National Center for Atmospheric Research, Boulder, Colorado.

13. Kesel, P. G. and Winninghoff, F. J., 1970: Developing an Atmospheric Primitive Equation Model for Operational Use by the United States Navy, Fleet Numerical Weather Central, Monterey Report.

14. Langlois, W. E. and Kwok, H. C. W., 1969: Description of the Mintz-Arakawa Numerical General Circulation Model, Technical Report No. 3, Department of Meteorology, University of California, Los Angeles.

15. Lavoie, R. L. and Wiederanders, C. J., 1968: Objective Wind Forecasting Over the Tropical Pacific, Scientific Report No. 1, Hawaii Institute of Geophysics.

16. Lewis, J. M., 1972: Adjustment of surface wind and pressure by Sasaki's variational matching technique, To be published in the Journal of Applied Meteorology.

17. Sasaki, Y., 1958: An objective analysis based on the variational method, Journal Meteorological Society of Japan, 36, 77-88.

18. Shapiro, R., 1971: The use of linear filtering as a parameterization of atmospheric diffusion, Journal of Atmospheric Sciences, 28, 4, 523-531.

19. Steinbruck, C. G., 1971: Some Design Experiments Toward an Operational Primitive Equation Model for the Tropics, M. S. Thesis, Naval Postgraduate School.

INITIAL DISTRIBUTION LIST

		No. Copies
1.	Defense Documentation Center Cameron Station Alexandria, Virginia 22314	2
2.	Library, Code 0212 Naval Postgraduate School Monterey, California 93940	2
3.	Dr. R. L. Elsberry Department of Meteorology, Code 51Es Naval Postgraduate School Monterey, California 93940	8
4.	Lieutenant Rodger A. Langland Fleet Numerical Weather Central Naval Postgraduate School Monterey, California 93940	4
5.	Dr. R. T. Williams Department of Meteorology, Code 51Wu Naval Postgraduate School Monterey, California 93940	1
6.	Dr. R. L. Haney Department of Meteorology, Code 51Hy Naval Postgraduate School Monterey, California 93940	1
7.	Dr. J. M. Lewis Fleet Numerical Weather Central Naval Postgraduate School Monterey, California 93940	1
8.	Lieutenant Gregory W. Svenheim Fleet Numerical Weather Central Naval Postgraduate School Monterey, California 93940	1
9.	Lieutenant Commander Charles G. Steinbruck USS MIDWAY (CVA-41) FPO, San Francisco, California 96601	1
10.	Naval Weather Service Command Washington Navy Yard Washington, D. C. 20390	1

11. Commanding Officer 1
Fleet Numerical Weather Central
Naval Postgraduate School
Monterey, California 93940

12. Officer-in-Charge 1
Environmental Prediction Research Facility
Naval Postgraduate School
Monterey, California 93940

13. Department of Meteorology, Code 51 1
Naval Postgraduate School
Monterey, California 93940

Security Classification

DOCUMENT CONTROL DATA - R & D

(Security classification of title, body of abstract and indexing annotation must be entered when the overall report is classified)

1. ORIGINATING ACTIVITY *(Corporate author)*

Naval Postgraduate School
Monterey, California 93940

2a. REPORT SECURITY CLASSIFICATION

Unclassified

2b. GROUP

3. REPORT TITLE

Some Numerical Aspects of Developing an Operational Primitive-Equation Model for the Tropics

4. DESCRIPTIVE NOTES *(Type of report and inclusive dates)*

Master's Thesis; March 1972

5. AUTHOR(S) *(First name, middle initial, last name)*

Rodger A. Langland

6. REPORT DATE: March 1972

7a. TOTAL NO. OF PAGES: 67

7b. NO. OF REFS: 19

8a. CONTRACT OR GRANT NO.

b. PROJECT NO.

c.

d.

9a. ORIGINATOR'S REPORT NUMBER(S)

9b. OTHER REPORT NO(S) *(Any other numbers that may be assigned this report)*

10. DISTRIBUTION STATEMENT

Approved for public release; distribution unlimited.

11. SUPPLEMENTARY NOTES

12. SPONSORING MILITARY ACTIVITY

Naval Postgraduate School
Monterey, California 93940

13. ABSTRACT

A barotropic primitive equation model on a global tropical grid using operational real data is used to test various boundary conditions and methods of initialization including numerical variational analysis. Comparisons of forecast accuracy are made between staggered and non-staggered grids.

All prediction models produce better verification statistics than persistence, with the staggered grid verifying better than the full grid. This appears to be a result of two-gridlength noise being of greater magnitude in the full grid model. Less altering of individual synoptic systems occurs in the variational analysis initialization compared to two forms of the nonlinear balance equation. As a result, non-divergent variational analysis input fields to the prediction models result in the best verification values.

DD FORM 1 NOV 65 1473 (PAGE 1)

S/N 0101-807-6811

Security Classification

A-31408

KEY WORDS	LINK A		LINK B		LINK C	
	ROLE	WT	ROLE	WT	ROLE	WT
Staggered grid						
Numerical variational analysis						
Nonlinear balance equation						
Nondivergent						
Prognosis verification						
No-flux boundaries						
Restoration boundaries						

Thesis
L2635 Langland
c.1
134443
Some numerical aspects of developing an operational primitive-equation model for the tropics.